IOPscience iopscience.iop.org

Home Search Collections Journals About Contact us My IOPscience

X-ray standing waves at surfaces

This article has been downloaded from IOPscience. Please scroll down to see the full text article.

2002 J. Phys.: Condens. Matter 14 4059

(http://iopscience.iop.org/0953-8984/14/16/301)

View the table of contents for this issue, or go to the journal homepage for more

Download details:
IP Address: 171.66.16.104
The article was downloaded on 18/05/2010 at 06:29

Please note that terms and conditions apply.

INSTITUTE OF PHYSICS PUBLISHING JOURNAL OF PHYSICS: CONDENSED MATTER

J. Phys.: Condens. Matter **14** (2002) 4059–4074 PII: S0953-8984(02)30346-1

X-ray standing waves at surfaces

Robert G Jones[1,5], A S Y Chan[1], M G Roper[1], M P Skegg[1], I G Shuttleworth[1], C J Fisher[2], G J Jackson[2], J J Lee[2], D P Woodruff[2], N K Singh[3] and B C C Cowie[4]

[1] School of Chemistry, University of Nottingham, Nottingham, NG7 2RD, UK
[2] Department of Physics, University of Warwick, Coventry, CV4 7AL, UK
[3] Department of Physical Chemistry, School of Chemistry, University of New South Wales, Sydney 2052, Australia
[4] CLRC Daresbury Laboratory, Warrington, WA4 4AD, UK

E-mail: robert.g.jones@nottingham.ac.uk

Received 31 October 2001, in final form 14 December 2001
Published 11 April 2002
Online at stacks.iop.org/JPhysCM/14/4059

Abstract

Adatoms immersed in an x-ray standing wave at a surface betray their position within the wave by the way they absorb the x-rays; feebly when positioned at the nodes, strongly when positioned at the antinodes. The elemental (and chemical) identity of the adatoms are easily monitored using the binding energies of the photoelectron or Auger electron emissions, while the intensities of these emissions provide the information needed to determine the atomic positions relative to the crystalline substrate which formed the standing wave. By using normal incidence Bragg diffraction to generate the standing wave, the technique is applicable to the rather imperfect crystalline samples and standard manipulators used in most surface science studies. Examples of structural studies from a range of systems will be drawn from recent work carried out at the SRS in Daresbury to illustrate the strengths, and weaknesses, of this structural technique. Specifically, the structure of reactive intermediates (SiH_x) formed by chemical reaction of silane on Cu(111); the structure of a physisorbed molecule ($ClCH_2CH_2F$) on Cu(111); an example of how chemically shifted Auger peaks may be useful for chemical shift XSW (chloroform on a chlorinated copper surface), and a system which presents many difficulties when studied by this technique, methyl thiolate on Au(111).

(Some figures in this article are in colour only in the electronic version)

1. Introduction

X-ray standing wave (XSW) analysis uses Bragg reflection of x-rays from an (hkl) set of crystal planes in the substrate to establish a standing wave at the surface with which to determine the

[5] Author to whom any correspondence should be addressed.

 © 2002 IOP Publishing Ltd Printed in the UK

positions of surface atoms. The normal incidence version [1], NIXSW, restricts the x-rays to being incident along the normal to the (hkl) set of planes, which has the great advantage of allowing the XSW technique to be applied to almost all single-crystal samples encountered in surface science (most metal crystals are too imperfect to be used at any angle other than normal incidence).

XSW is a structural technique [2,3], applicable to many situations, with an accuracy which can be as good as $\approx$0.02 Å. Although it requires single-crystal samples to establish the standing wave, the surface under study need not have long-range order. It is element specific, meaning the position of each element on a surface can be determined independently, and by using chemical shifts in either the x-ray photoelectron spectrum or the Auger electron spectrum, it can be made chemically specific too. The technique is exceedingly good at identifying high-symmetry adsorption sites, and it is this aspect which we concentrate upon in this paper.

XSW provides just two structural parameters (the coherent position, d_{hkl}, and the coherent fraction, f_{hkl}) per element (or chemically shifted component of an element) per (hkl) set of planes used. d_{hkl} and f_{hkl} are related to the distribution of positions of the species under study with respect to the (hkl) scatterer planes. At least two sets of planes, $(h_1k_1l_1)$ and $(h_2k_2l_2)$, one of which lies parallel to the sample surface, and the other(s) at an angle to it, are needed to triangulate the adatom positions in three dimensions. It is this aspect which is the strength of the technique, as the pairs of d and f values are model independent, and if the species being studied resides in a single high-symmetry site, then the experimental d and f values from the different (hkl) planes can be used to show that only that adsorption site is possible. However, this aspect is also a weakness, as the limited number of experimentally available sets of (hkl) planes means a small number of experimental d and f pairs, and if the element is in a multiplicity of sites, there may be insufficient data to determine all the atomic positions.

Four adsorption systems will be used to illustrate the technique of NIXSW. Silyl (SiH_x) adsorption on Cu(111) is rather straightforward experimentally and is illustrative of a surface intermediate which has been stabilized using kinetic control at low temperature. Chlorofluoroethane, $ClCH_2CH_2F$, (CFE) adsorption on Cu(111) is experimentally rather more complex and demonstrates how the positions of two elements (Cl and F) in a physisorbed system may be determined simultaneously. Chloroform ($CHCl_3$) adsorption on a Cu(111) surface pre-covered with chemisorbed chlorine, is used to illustrate how chemical shifts can be used to measure separate XSW data from chemically distinct states of the same element (chlorine). Finally, dimethyldisulphide, CH_3SSCH_3, (DMDS) on Au(111) is used to show how even an experimentally difficult system can be studied using NIXSW.

2. The x-ray standing wave technique

Two waves of the same wavelength which overlap in space will form a standing wave provided they have a fixed phase relationship. In principle any method of establishing this situation can be used for XSW studies, (such as interference between the incident and reflected beam for grazing incidence x-ray reflection from a mirror [4]) but in this paper Bragg reflection from a single crystalline sample is the method used.

In Bragg x-ray diffraction the incident and diffracted beams are related by Braggs law:

$$n\lambda = 2D_{hkl}\sin\theta \tag{1}$$

where n is the order of diffraction, λ is the x-ray wavelength, D_{hkl} is the layer spacing of the x-ray scatterer plane with Miller index (hkl) and θ is the angle between the (hkl) plane and the x-ray beam. One can achieve Bragg x-ray diffraction by fixing λ, i.e. the photon energy E) and varying θ, or fixing θ and varying λ (i.e. E). For NIXSW, θ is fixed at 90°, $\lambda = 2D_{hkl}$,

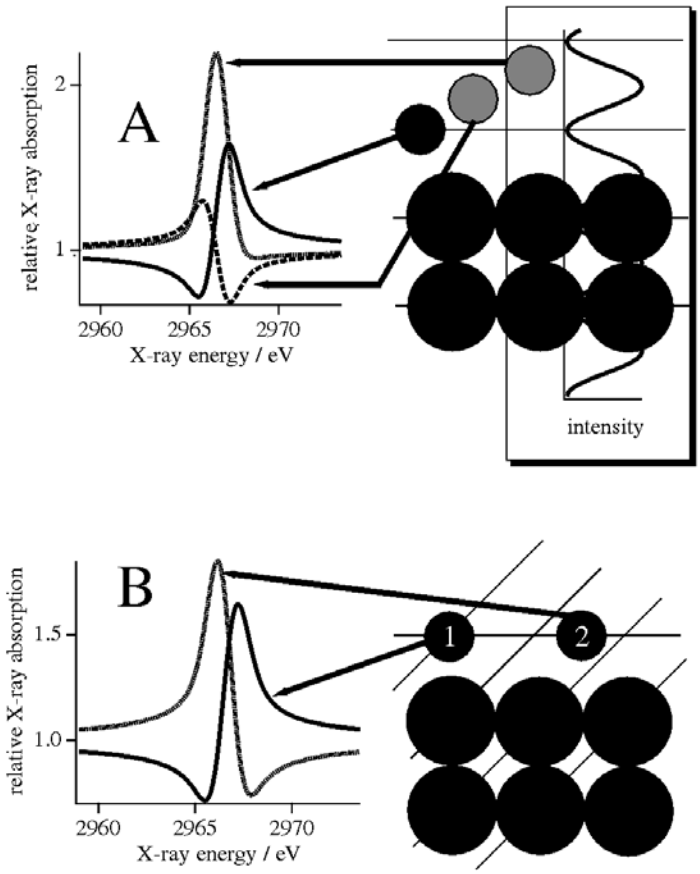

Figure 1. (a) Schematic showing three adatoms at positions of 0 (or 1), 1/3 and 2/3 of D_{h1k1l1} above the $(h_1k_1l_1)$ scatterer planes which are parallel to the surface, and their associated XSW curves. The spatial intensity of the XSW is also indicated for the low-energy side of the scans. (b) Schematic showing how an angled set of $(h_2k_2l_2)$ planes can be used to determine the adsorption site of an adatom which is at a fixed height above the surface. Atom 1 lies in an atop site and is located on the angled planes, atom 2 lies in a hollow and is mid-way between the angled planes.

and hence a standard manipulator (with a low accuracy in θ) can be used to hold the sample because the highly accurate x-ray monochromator is used to scan E.

Away from the Bragg condition the surface atoms experience a travelling x-ray wave, defined as having a relative intensity of 1, leading to x-ray absorption at the surface atoms (relative x-ray absorption of 1) and hence photoelectron emission, with subsequent decay of the core holes giving Auger electron emission or fluorescence x-ray emission. As the Bragg condition is approached by varying E (from the low-energy side) or θ a diffracted wave forms due to scattering from the top several microns of the substrate crystal. Using dynamical theory, it can be shown that the phase relationship between the incident and the diffracted beam at this energy is such that they form a standing wave which has its nodes on the (hkl) scatter planes, and its antinodes half way between the planes, figure 1(a). If the diffracted beam were of the same amplitude as the incident beam, then the intensity at the antinodes would be $4\times$ the travelling wave intensity, while the intensity at the nodes would be zero. This is not realised in practice, but it provides a useful way of understanding the shapes of XSW curves. As the Bragg condition is traversed (moving to higher photon energy), the phase relationship between

the incident and the diffracted beam alters such that the standing wave moves by $D_{hkl}/2$ until the antinodes are on the scatterer plane and the nodes are half way between. Further scanning of E or θ then causes the diffracted beam amplitude to drop to zero and the system returns to a simple travelling wave passing through the surface. For a photon energy of ≈3000 eV ($\lambda \approx 4$ Å) the XSW exists over about an eV, which is broadened to a few eV by the finite resolution of the x-ray monochromator used.

Adatoms at the sample surface are immersed in the XSW field at a particular position, z_{h1k1l1}, relative to the scatterer layer spacing, D_{h1k1l1}, which is also the periodicity of the intensity of standing wave. An atom at a node will only weakly absorb the x-rays, while one at an antinode will strongly absorb. By monitoring the relative x-ray absorption via photoelectrons, Auger electrons or x-ray fluorescence photons, a particular shape of relative absorption versus E is obtained. A different shape is obtained for each z_{h1k1l1}/D_{h1k1l1}, figure 1(a), and this allows the atomic position relative to the $(h_1k_1l_1)$ scatterer planes to be determined. Note that as the standing wave has a periodicity of D_{h1k1l1} the position can only be determined *within that periodicity* (i.e. the same result is obtained for the same position within every period of the standing wave intensity). By carrying out the experiment with a second (or possibly more) set of planes, $(h_2k_2l_2)$, which lie at an angle to the first set, values of z_{h2k2l2}/D_{h2k2l2} can be obtained for the positions of the adatoms relative to these planes, which allows the complete position of adsorbates to be triangulated for specific sites on the surface, figure 1(b). For the (111) surfaces of fcc crystals the (111) and $(\bar{1}11)$ scatterer planes are most frequently used as one lies parallel to the sample surface, giving distances perpendicular to it, while the other lies at an angle of 70.5° to the surface, figure 3, giving distances which have a predominantly horizontal component. Both planes have the same $D_{\{111\}}$ distance.

The experimental XSW curve is analysed in terms of the coherent position, d_{hkl}, and the coherent fraction, f_{hkl}. Provided the adatoms are all absorbed at just one position, z_{hkl}, relative to the (hkl) planes, then $d_{hkl} = z_{hkl}$ and $f_{hkl} = 1$. At the other extreme, for adatoms adsorbed with equal probability across all possible positions, $0 \leqslant z_{hkl}/D_{hkl} \leqslant 1$, then $f_{hkl} = 0$ and d_{hkl} is indeterminate. Between these extremes, where the species have either a discrete or a continuous distribution of z_{hkl} values (each with its own individual coherent fraction, which we call the site order parameter (s_{hkl})), a vector sum of the z_{hkl}, s_{hkl} pairs provides the single f and d pair which is determined experimentally for a given (hkl) set of planes [3, 5]. The distribution of z_{hkl} values may be due to a static variation (e.g. different adsorption sites leading to different distances relative to the (hkl) planes) or dynamic motion (e.g. vibrational motion about a particular mean distance relative to the (hkl) planes). Clearly it may not be possible to move from a limited number of experimental f, d pairs for different (hkl) planes, to a greater number of z, s pairs representing the complete surface structure.

NIXSW experiments require high-intensity, tuneable x-rays, which are only available at second (and later) generation synchrotron radiation sources. All the experiments described in this paper were carried out on beam line 6.3 of the SRS at Daresbury Laboratory, UK XSW scan times were between 30 min and several hours. On third generation synchrotrons these times can be reduced to just seconds

3. Cu(111)-(3 × 3)-SiH$_x$

Silane, SiH_4, reacts with Cu(111) at 425 K to produce a $(\sqrt{3}\times\sqrt{3})R30°$-$Cu_2Si$ surface alloy [6] which has recently been studied using NIXSW [7]. For adsorption at lower temperature, 140 K, the reactive silyl intermediates (SiH_x) can be stabilized on the surface and exhibit a (3 × 3) surface mesh as observed with helium atom scattering, HAS, but which appears as a $(\sqrt{3} \times \sqrt{3})R30°$ structure when observed with low-energy electron diffraction, LEED. This surface is thought to consist of 1/3 ML of SiH_3 species and 1/9 ML SiH or Si species. Note

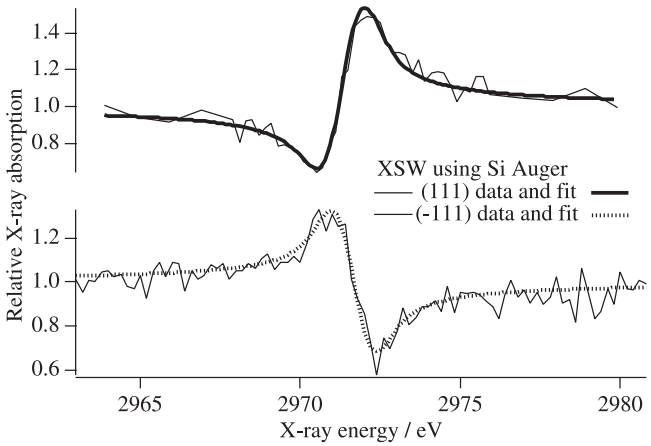

Figure 2. NIXSW curves using the Si Auger transition at 1619 eV for the (111) and ($\bar{1}$11) Bragg reflections from the silyl covered surface. The fitting parameters used were: (111), $d/D_{\{111\}} = 0.95$, $f = 0.88$; ($\bar{1}$11), $d/D_{\{111\}} = 0.66$, $f = 0.82$.

that LEED can only 'see' the silicon adatoms, which have a $(\sqrt{3} \times \sqrt{3})R30^\circ$ arrangement, because electron scattering from hydrogen is weak, making the hydrogens invisible. HAS, however, is sensitive to the difference between the SiH_3 and SiH (or Si) groups, and so it can 'see' the full (3×3) surface mesh; see figure 4.

In the NIXSW experiments we used the 1619 eV kinetic energy (KE) silicon Auger peak to monitor the relative x-ray absorption versus photon energy. At each photon energy the signal at the top of the silicon Auger peak was measured (the 'on' signal), and the signal at the foot of the peak, a few eV to higher KE was also measured (the 'off' signal). The relative x-ray absorption was then found by simply subtracting the 'off' signal from the 'on' signal to get the intensity of the Auger peak itself. This signal was then normalized, using the measured incident x-ray intensity, such that the relative x-ray absorption outside of the standing wave region (i.e. the wings of the XSW scan) was 1.0 (see figures 1 and 2). Substrate data, in this case XSW curves monitored using the copper Auger peak at 920 eV, were also measured at the same time as the silicon data. Substrate XSW curves may also be measured by monitoring the secondary electron yield from the sample at almost any KE, or indeed by monitoring the total electron yield via the drain current to earth from the sample.

Figure 2 shows the XSW data for silicon in the adsorbed SiH_x species, obtained using the (111) and ($\bar{1}$11) scatterer planes. The fitting parameters used were d and f, as described above, the experimental broadening of the XSW curves, σ, due to the resolution of the x-ray monochromator, and the Bragg energy, E_0. As the copper Auger electron signal is $\approx$95% dominated by the bulk structure of the substrate, σ and E_0 are usually obtained by fitting the copper substrate XSW curve by fixing $d_{\{111\}} = D_{\{111\}} = 2.08$ Å, the known bulk layer spacing for the $\{111\}$ planes, and obtaining the best fit for σ, E_0 and f. The non structural parameters, σ and E_0, are then transferred to the silicon analysis to obtain the best fit by varying just d and f. (Note that the experimental values of E_0 and σ vary slightly from one scan to the next, due to the changing power loading of the white synchrotron beam on the monochromator crystals with time. It is therefore normal to take substrate (Cu) and adlayer (Si) data at the same time, so that E_0 and σ can be determined from the known substrate structure and transferred as known quantities to the analysis of the unknown adlayer structure).

Table 1 shows the values of d and f obtained by fitting several silicon and copper data sets for several surface preparations. As expected, the fitting parameters for the (111) and the

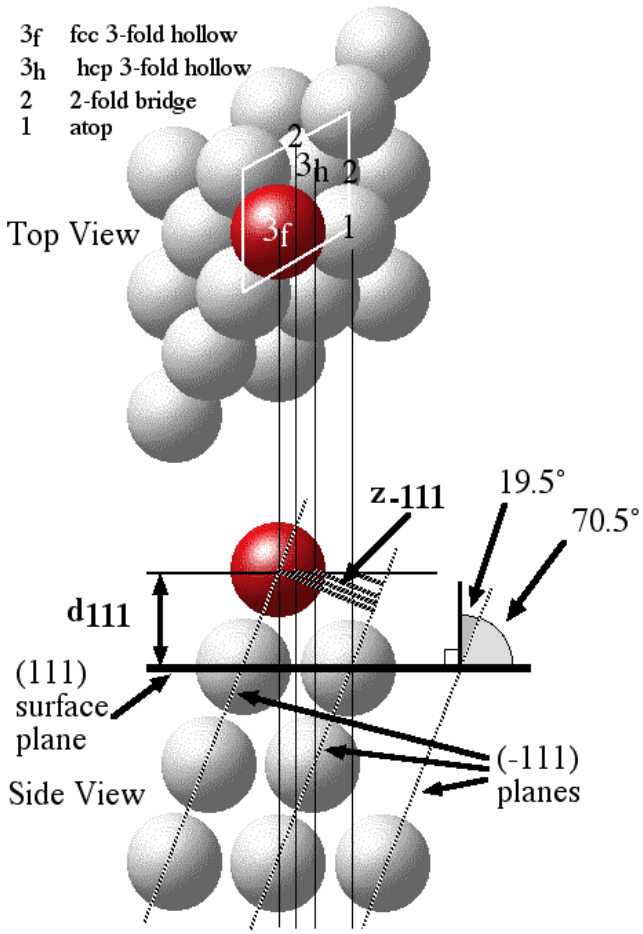

Figure 3. Top and side views of an fcc crystal, showing how the distance $z_{\bar{1}11}$ of an adatom (dark sphere) from the inclined $(\bar{1}11)$ planes varies for different adsorption sites for a fixed distance d_{111} from the (111) scatterer planes which are parallel to the surface. The four different $z_{\bar{1}11}$ distances corresponding to those calculated using equations (2)–(5) are also shown.

$(\bar{1}11)$ copper data are the same, because the copper atoms reside on the scatterer planes for both. Rather surprisingly, the best fit was obtained for $d = 2.04$ Å, slightly lower than the bulk value of 2.08 Å, and the coherent fraction of $\approx$0.82 was lower than the usual value of $\approx$0.85. The reason for this slight discrepancy is not understood.

For the silicon atoms, the (111) data shows them to be 1.98 ± 0.04 Å above the surface scatterer plane with a coherent fraction of 0.88 ± 0.03. As this is close to the coherent fraction of the substrate, it means that all the silicon atoms are well ordered at a single position relative to the (111) planes. The $(\bar{1}11)$ silicon data has a coherent fraction of 0.79, again rather close to the substrate value, so all the silicon atoms are at a single position of 1.39 ± 0.04 Å from the $(\bar{1}11)$ planes.

Figure 3 illustrates the procedure used to determine the adsorption site of the silicon using the experimental d_{111} and $d_{\bar{1}11}$ values. The distance of the adatom above the substrate surface atomic plane is $z_{111} = d_{111} + nD_{111}$, where n is an integer, as we do not know how many empty (111) planes there are between the adatom and the surface substrate atoms. On Cu(111) there

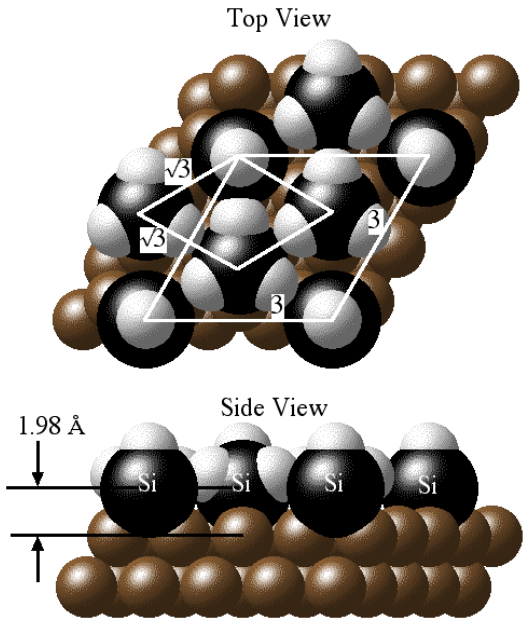

Figure 4. Hard sphere model of the Cu(111)-(3×3)-SiH_x surface using the atomic radius for copper (1.278 Å) and the van der Waals radii for Si (2.0 Å) and hydrogen (1.2 Å). All silicon atoms are in hcp 3-fold hollows at a distance of 1.98 Å from the surface copper plane. Two possible SiH_x species, SiH_3 and SiH, are shown, together with the (3 × 3) and ($\sqrt{3} \times \sqrt{3}$)$R30^\circ$ surface meshes observed by HAS and LEED, respectively. The number and positions of the hydrogens are speculative.

Table 1. NIXSW data for Cu(111)-(3 × 3)-SiH_x. Note. The experimentally (Exptl) determined coherent positions (d) and coherent fractions (f) are shown for each Bragg reflections using the indicated transition, the error in the least significant figure is shown in brackets. Calculated (Calc) values of $d_{\bar{1}11}$ for silicon, using $z_{111} = 1.98$ Å, and the associated maximum value of f, are also shown for ($\bar{1}11$) silicon data when the Si is positioned in various high-symmetry sites.

Transition	Reflection	Exptl d/Å and f	Calc $d_{\bar{1}11}$ for atop	Calc $d_{\bar{1}11}$ for bridge	Calc $d_{\bar{1}11}$ for hcp 3-fold hollow	Calc $d_{\bar{1}11}$ for fcc 3-fold hollow
Cu Auger	(111)	2.04(4) 0.82(1)				
Cu Auger	($\bar{1}11$)	2.04(4) 0.81(1)				
Si Auger	(111)	1.98(4) 0.88(3)				
Si Auger	($\bar{1}11$)	**1.39(4)** 0.79(3)	0.66 1	1.70 0.33	**1.36** 1	2.05 1

are four high symmetry sites, atop, hcp 3-fold hollow (copper atom two layers down directly below adatom), fcc 3-fold hollow (copper atom three layers down directly below adatom), and 2-fold bridge. The atop and 3-fold hollow sites have a single position, $z_{\bar{1}11}$, with respect to the angled ($\bar{1}11$) planes, so $d_{\bar{1}11}$ can be equated with $z_{\bar{1}11}$ directly and the value of f is expected to be high (maximum theoretical value of 1, but experimentally it will be close to the substrate f value) if the atoms reside in one of these sites. The bridge sites occupy two distances relative

to the ($\bar{1}11$) planes with a population ratio of 2:1, which when combined correctly [3,5] gives a single value of $d_{\bar{1}11}$ with a maximum theoretical value of $f = 0.33$.

For $n = 0$ ($z_{111} = d_{111}$) the equations used to calculate $z_{\bar{1}11}$ from d_{111} for adatoms in different adsorption sites are as follows:

atop	$z_{\bar{1}11} = d_{111} \sin 19.5^\circ$	(2)
2-fold bridge	1/3 pop at $z_{\bar{1}11} = d_{111} \sin 19.5^\circ$	
	2/3 pop at $z_{\bar{1}11} = (d_{111} + 3D_{111}/2) \sin 19.5^\circ$	(3)
fcc 3-fold hollow	$z_{\bar{1}11} = (d_{111} + 2D_{111}) \sin 19.5^\circ$	(4)
hcp 3-fold hollow	$z_{\bar{1}11} = (d_{111} + D_{111}) \sin 19.5^\circ$.	(5)

If, for chemical reasons, it is decided that $n = 1$ ($z_{111} = d_{111} + D_{111}$), the equations for the sites become atop (5), fcc 3-fold (2), hcp 3-fold (4), and if it is decided that $n = 2$ ($z_{111} = d_{111} + 2D_{111}$) the equations for the sites become atop (4), fcc 3-fold (5), hcp 3-fold (2). This is equivalent to lowering the surface copper plane by removing one, or two, (111) layers of copper atoms from below the adatom in figure 3.

Table 1 shows the calculated values of $d_{\bar{1}11}$ and $f_{\bar{1}11}$ using the experimental value of d_{111}. Clearly only one calculated value for $d_{\bar{1}11}$ matches the experimental value (1.36 and 1.39 Å). We can therefore state that all the silicon atoms in the silyl phase are located in the hcp 3-fold hollows, and not in any other high-symmetry site. Figure 4 shows a hard sphere model for the surface. Both silicon species on the surface, SiH_3 and SiH/Si, occupy the same type of site, and have the same bond length (≈2.5 Å) to within the resolution of this experiment. This bond length agrees well with the sum of the copper atomic radius and the silicon covalent radius (1.278 + 1.17 = 2.448 Å).

4. 1-chloro-2-fluoroethane (CFE) on Cu(111)

The adsorption sites of physisorbed molecules are of fundamental interest as they constitute the precursor states to many chemical reactions at surfaces. Here we have studied a physisorbed halocarbon which has been used in surface dynamics experiments involving dissociative electron attachment [8], and hence a knowledge of its surface structure is necessary. CFE adsorbs molecularly on Cu(111) at 100 K [9]. The chlorine XSW scan can be monitored very simply using 'on' and 'off' signals for the chlorine $KL_{2,3}L_{2,3}$ Auger transition at 2382 eV. However, the fluorine XSW scans pose a problem, as the Auger peak at 647 eV is too weak to be of use. The F 1s photoelectron peak, at a KE of about 2286 eV in these experiments, can be employed to measure the XSW scan, using 'on' and 'off' measurements, but a certain amount of data manipulation is required to eliminate the undesirable effect caused by the fluorine photoelectron peak passing over a weak $KL_1L_{2,3}$ chlorine Auger peak [9].

When using photoelectron peaks measured using an angle resolving electron energy analyser to monitor the relative x-ray absorption, a correction has to be applied in the fitting procedure used to determine f and d if the binding energy (BE) of the level involved is very much less than the x-ray energy of the standing wave; failure to do this leads to unrealistic values of f (e.g. >1) and inaccuracies in d. The problem is caused by a breakdown in the dipole approximation for photoemission when the size of the orbital becomes significant relative to the x-ray wavelength [10, 11], XSW being particularly sensitive to this effect.

Very briefly, the problem is as follows. In the dipole approximation, for an s → p transition (as here), the outgoing photoelectron wave is a double-lobed p wave aligned with the electric vector of the x-ray wave. This photoelectron angular distribution, part of which is measured by the electron energy analyser, is the same for both the incident beam, and for the diffracted beam travelling in the diametrically opposite (180°) direction (for NIXSW). NIXSW scans

have three regions: a travelling incident wave region (to lower energy of the standing wave), a middle region with two oppositely propagating waves (the standing wave region), and a second travelling wave region (to higher energy of the standing wave region). As noted above, XSW scans have to be normalized and this is done using 1.0 as the intensity of the incident travelling wave to higher and lower energy of the standing wave region. As the photoelectron angular distributions are the same for all three regions (in the dipole approximation) this normalization is valid for all three regions. However, when the dipole approximation breaks down, the photoelectron angular distribution is (usually) bent forward in the direction of motion of the photons. We now have a forward/backward asymmetry, and the measured photoelectron intensity will depend on whether the x-ray has a component which is propagating towards, or away from, the electron energy analyser. Within the standing wave region the effects of the forward and backward propagating waves almost cancel each other out (i.e. overall the behaviour is similar to the dipole approximation), but outside of this region, (above and below the standing wave region), it has an unfettered effect and the photoelectron intensity is not what it would be in the dipole approximation (often up to 20–30% lower). So if the NIXSW scan is normalized using the regions outside of the standing wave region, the normalization is incorrect for the standing wave region itself. To deal with this, a forward/backward asymmetry parameter, Q, is introduced into the theory, such that the wings of the NIXSW scan are normalized to 1.0 as usual and the Q value compensates for the error this introduces into the normalization within the standing wave region. Q has to be determined in separate experiments.

For the fluorine 1s photoelectron peak used here (BE = 686 eV) at a photon energy of ≈3000 eV, the breakdown in the dipole approximation is significant, requiring a correction factor, $Q = 0.255$. Data measured using Auger electrons require no corrections ($Q = 0$).

The NIXSW scans for chlorine and fluorine using the (111) and ($\bar{1}11$) Bragg reflections are shown in figure 5. It is immediately obvious that the pair of XSW scans for Cl are very similar to the pair for F, implying a similar adsorption site for both halogens. Fitting parameters are shown in table 2. The values of d_{111} found for the two halogens (0.98 and 0.94 Å) are far too small for chemically realistic bond lengths, so the true layer spacings must be $z_{111} = d_{111}+D_{111}$, i.e. 3.06 Å for chlorine and 3.02 Å for fluorine.

The highest coherent fraction (0.48) occurs for chlorine in the (111) reflection, but this is substantially lower than the substrate copper value of ≈0.85. This may be due to a large amplitude vibration perpendicular to the sample surface, or static disorder due to a range of orientations on the surface, or possibly contributions from both. The next highest f value occurs for fluorine in the (111) reflection, implying an even bigger vibrational amplitude or range of static disorder. The f values of both halogens in the ($\bar{1}11$) reflection are very low, ≈0.25.

Using the same procedure as that used for the SiH_x species, values of $z_{\bar{1}11}$ and hence $d_{\bar{1}11}$ can be calculated for high symmetry adsorption sites using the experimental values of d_{111}, for comparison with the experimental values of $d_{\bar{1}11}$, table 2. Note that the equation which corresponds to a particular site (see above) changes because the distance between the adatom and the substrate surface layer is $d_{111}+D_{111}$. For chlorine there is excellent agreement between the $d_{\bar{1}11}$ values for the atop site (0.94 and 1.02 Å). For fluorine the atop site also shows the best agreement (0.83 and 1.01 Å), but it is not quite as good as for chlorine.

Figure 6 shows a hard sphere model of the molecule on the surface. If the chlorine end of the molecule is positioned in an atop site, with the molecule orientated such that the Cl...F axis lies along the $\sqrt{3}$ direction in the surface, figure 6, then the F atom lies almost directly above another atop site. Using van der Waals diameters in the model, it can be seen that the chlorine end is in contact with the surface atom, whereas the fluorine end is not. Clearly the bonding is dominated by the Cl end, not the F end. The sum of the Cu atomic radius (1.278 Å) and the chlorine van der Waals radius (1.80 Å) gives a Cu...Cl physisorption bond length of

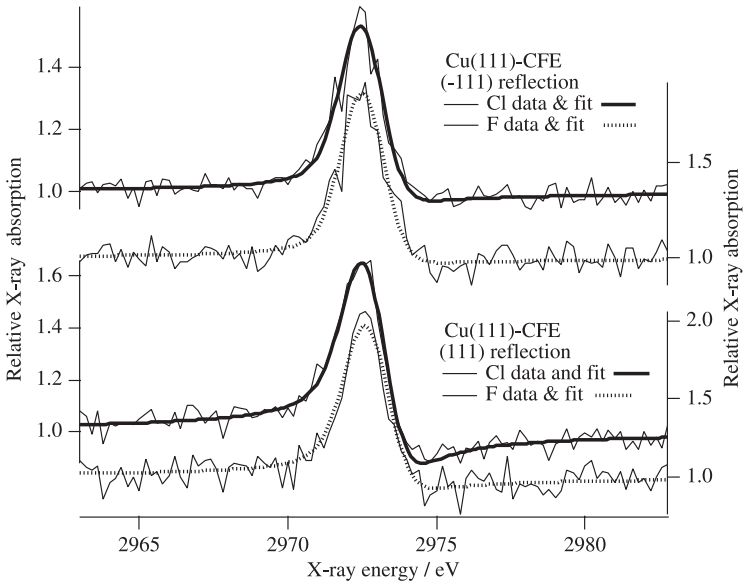

Figure 5. Chlorine and fluorine NIXSW curves are shown for one layer of CFE adsorbed on Cu(111) at 100 K using the (111) and ($\bar{1}11$) Bragg reflections. The Cl and F data were obtained by monitoring the $KL_{2,3}L_{2,3}$ Auger peak and the 1s photoelectron peak, respectively. Fitting parameters for the (111) data were: for Cl, $d/d_{\{111\}} = 0.48$, $f = 0.57$; for F, $d/d_{\{111\}} = 0.44$, $f = 0.41$. Fitting parameters for the ($\bar{1}11$) data were: for Cl, $d/d_{\{111\}} = 0.46$, $f = 0.21$; for F, $d/d_{\{111\}} = 0.44$, $f = 0.20$.

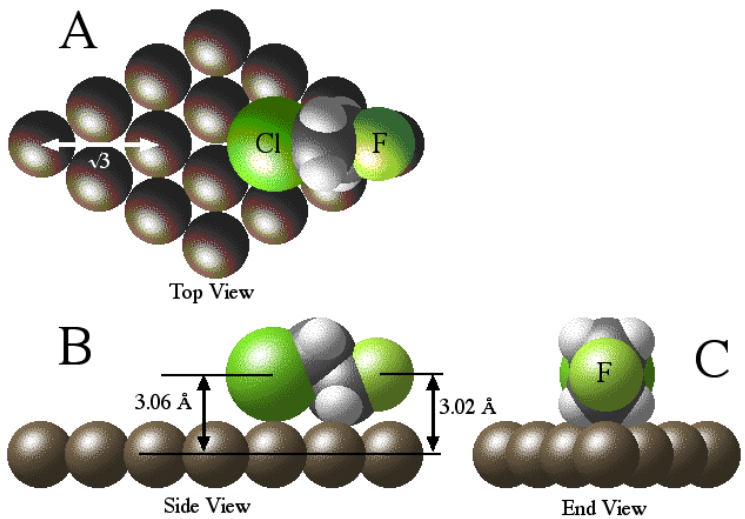

Figure 6. Top A, side B and end C, views of 1-chloro-2-fluoroethane adsorbed on Cu(111) with the chlorine in an atop position, and the fluorine close to an atop position. The molecule is shown in the anti conformation with the Cl–C–C–F plane aligned perpendicular to the surface. The atoms are shown with hard sphere radii equal to their van der Waals radii. The experimentally determined heights of the two halogens are also shown. The positioning of the two CH_2 groups is speculative.

Table 2. NIXSW data for Cu(111)-CFE. Note. The experimentally (Exptl) determined coherent positions (d), $d + D_{\{111\}}$ positions (in square brackets) and coherent fractions (f) are shown for each Bragg reflection using the indicated transition, the error in the least significant figures is shown in round brackets. Calculated (Calc) values of $d_{\bar{1}11}$ for chlorine using $d_{111} = 0.98$ Å, and for fluorine using $d_{111} = 0.94$ Å, and the associated maximum values of f, are also shown for the ($\bar{1}11$) data when these atoms are positioned in various high symmetry sites. The Q values (see text) used in the analysis of the fluorine 1s data are also shown.

Transition	Reflection	Exptl d/Å $[d + D_{\{111\}}]$/(Å) f	Calc $d_{\bar{1}11}$ for atop	Calc $d_{\bar{1}11}$ for bridge	Calc $d_{\bar{1}11}$ for hcp 3-fold hollow	Calc $d_{\bar{1}11}$ for fcc 3-fold hollow	Q
Cl Auger	(111)	0.98(6) [3.06(6)] 0.48(10)					
Cl Auger	($\bar{1}11$)	**0.94(6)** — 0.24(4)	**1.02(2)** 1	2.06(2) 0.33	1.72(2) 1	0.33(2) 1	
F 1s	(111)	0.94(10) [3.02(10)] 0.37(7)					0.255
F 1s	($\bar{1}11$)	**0.83(15)** — 0.29(10)	**1.01(5)** 1	2.05(5) 0.33	1.70(5) 1	0.32(5) 1	0.255

3.078 Å, in very close agreement with the experimentally determined bond length of 3.06 Å. The low coherent fractions for the ($\bar{1}11$) reflection can now be better understood as being due to the molecule having a large degree of freedom parallel to the surface, but with the average positions of the Cl and F being atop.

5. Chemical shift x-ray standing wave (CSXSW) analysis

Chemical shifts in the 1s XPS spectra of phosphorous [12] and sulphur [13] chemically bonded to fluorine and oxygen respectively, have recently been used in XSW studies to determine the adsorption sites of these elements in two or more chemically distinct adsorbed species. In these studies the chemical shift was observed in an element (P or S) bonded to an electronegative species. Here we show that such studies can also be applied directly to the electronegative element, and that the chemical shift in the Auger electron peaks may be easier to use than the chemical shifts in the photoelectron peaks.

Chemisorbed chlorine (Cl_{chem}) can be formed on a Cu(111) surface by reaction at room temperature with chloroform ($CHCl_3$), forming a $(\sqrt{3} \times \sqrt{3})R30^\circ$ structure [14,15]. At 120 K chloroform molecules can then be physisorbed on to the $(\sqrt{3} \times \sqrt{3})R30^\circ$-Cl surface, thus providing chlorine in a second, molecular, environment, Cl_{mol} [16]. Figure 7 shows energy distribution curves (EDC) for the chlorine 1s photoelectron peak at a KE of ≈128 eV, and the high energy $KL_{2,3}L_{2,3}$ Auger electron peak at a KE of ≈2382 eV [17] (calculated energy 2376 eV [18]), both obtained using a photon energy of ≈2945 eV (which is close to the NIXSW energy for {111} Bragg reflections from copper). For the chemisorbed chlorine, Cl_{chem}, a single-photoelectron peak and a single-Auger-electron peak were observed using high-resolution (low pass energy) on the concentric hemisphere electron energy analyser. For

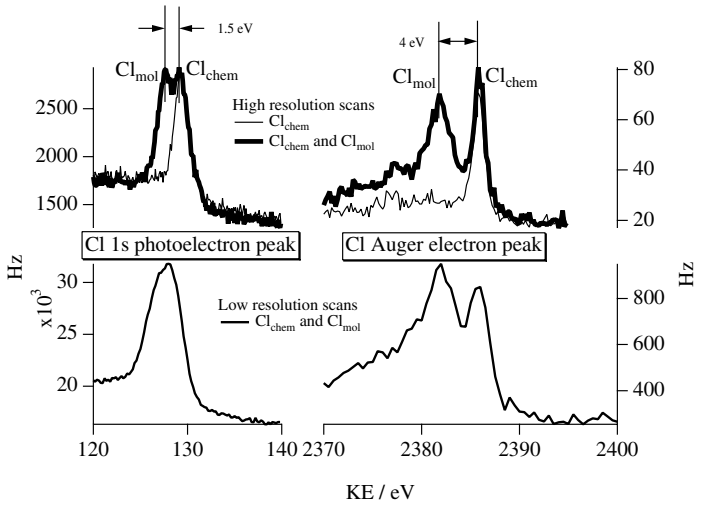

Figure 7. EDCs for the chlorine 1s photoelectron peak at ≈128 eV KE, and the chlorine $KL_{2,3}L_{2,3}$ Auger electron peak at ≈2382 eV KE, are shown for two surfaces: Cl_{chem}, where chlorine is chemisorbed in a $(\sqrt{3} \times \sqrt{3})R30^\circ$-Cl structure, and Cl_{chem} and Cl_{mol} where chlorine within molecular chloroform ($CHCl_3$), Cl_{mol}, has been adsorbed on the Cl_{chem} surface. The high-resolution scans (CHA pass energy 22 eV), clearly show the Cl_{chem} and Cl_{mol} components for both peaks. The low-resolution scans (CHA pass energy 90 eV) used for NIXSW analysis, illustrates how the smaller shift for the photoelectrons causes coalescence into a single peak.

chloroform ($CHCl_3$) molecularly adsorbed onto the $(\sqrt{3} \times \sqrt{3})R30^\circ$-Cl surface, Cl_{mol}, a chemically shifted photoelectron peak (≈1.5 eV to lower KE) and a chemically shifted Auger peak (≈4 eV to lower KE) were observed. The chemical shift of the Auger peak is almost three time that of the photoelectron chemical shift. In principle either the photoelectron peaks or the Auger electron peaks could be used to distinguish the relative x-ray absorption of chlorine in the two states. However, it is clear from figure 7 that when a low resolution (high pass energy) is used on the CHA to increase the signal, and hence improve the signal to noise ratio obtained in a NIXSW scan, the two species merge into one peak for the 1s photoelectron spectra, whereas the Auger peaks are still clearly distinguishable. It is thus easier to use the Auger peaks to carry out chemical shift XSW. An analysis of the adsorption structure of chloroform on the chlorinated Cu(111) surface is currently in progress using these peaks.

Large Auger electron chemical shifts such as these are to be found in transitions where all three levels are relatively strongly bound [19] (for Cl, K = 2823 eV, $L_{23} \approx 201$ eV). Auger transitions involving shallower levels, such as the chlorine 181 eV, LVV transition, tend not to show such large chemical shifts.

6. Dimethyldisulphide (DMDS) adsorption on Au(111)

At present there is great interest in the formation and use of 'self-assembled monolayers' (SAMs) on gold surfaces [20, 21], usually grown from dilute solutions of alkyl thiols onto evaporated gold films on glass substrates. In this section we show in detail why XSW measurements of sulphur on gold (carried out to determine the structure of the Au–S anchor of the SAM) are particularly difficult, resulting in only one XSW study [22] to date, which was interpreted as showing two distinct sulphur head group sites for decanethiol on Au(111).

We used DMDS to form methyl thiolate species on a Au(111) surface using the following reaction at 300 K:

$$CH_3SSCH_3(g) \rightarrow 2CH_3S(chem).$$

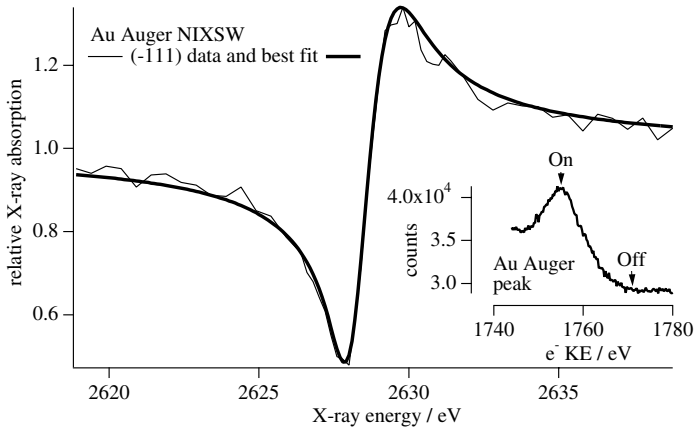

Figure 8. A ($\bar{1}11$) XSW scan obtained from an Au(111) sample using the Au Auger peak at ≈1772 eV. The fitting parameters were $d_{\bar{1}11}/D_{\{\bar{1}11\}} = 1.0$ (fixed), $f = 0.86$. Inset is the Au Auger peak with the 'on' and 'off' positions marked.

A disulphide was used to form the surface thiolate as we have found that small thiols (from butane thiol down to H_2S) undergo activated adsorption on Au(111), and hence have very low sticking probabilities at 300 K. The disulphide however, with its weaker S–S linkage, is more reactive and undergoes non-activated adsorption with a high sticking probability. The chemisorbed CH_3S formed a $(\sqrt{3} \times \sqrt{3})R30^\circ$ structure as observed by LEED, but as the incident electron beam destroyed the structure in a few seconds, LEED was only used after completion of a NIXSW experiment.

Figure 8 shows a gold ($\bar{1}11$) XSW curve obtained using the gold Auger peak at ≈1772 eV. The inset to the figure shows an EDC of the gold Auger peak, illustrating the 'on' and 'off' positions used in the scan. The Au ($\bar{1}11$) XSW curve looks rather different to those measured for substrates such as copper or nickel, with a substantial dip on the low-energy side, but only a small maximum on the high-energy side. This occurs because the {111} Bragg energy, at ≈2630 eV, lies between the gold M_{III} (2743 eV BE) and M_{IV} (2291 eV BE) absorption edges. Thus as the standing wave forms on the low-energy side of the XSW curve, the antinodes of the standing wave lie between the gold atoms and absorption is a minimum. On the high-energy side the standing wave moves such that the antinodes are now located on the gold atoms, and because the M_{IV} edge is only ≈340 eV below the Bragg energy, strong adsorption occurs at this position, reducing the x-ray intensity. The effects of absorption are automatically corrected by using the appropriate atomic scattering factors for gold (which have been adjusted for anomalous dispersion at the energy of the standing wave) in the fitting programme. The fit in figure 8 was obtained using $d_{111} = 2.3556$ Å (the bulk layer spacing of Au(111)), with a coherent fraction of 0.86, very similar to the values obtained with other metal crystals.

In figure 9 we show the EDC obtained from a clean Au(111) surface, together with an EDC from the same surface covered with a monolayer of SCH_3(chem). A large number of gold photoelectron and Auger electron peaks are visible, due to the large number of occupied energy levels in gold.

There are four possibilities for monitoring the relative x-ray absorption of sulphur in the methylthiolate; the K (1s) photoelectron peak (BE = 2472 eV), the L (2s, 2p) photoelectron peaks (BEs = 229 and 164/5 eV), the low-energy LVV sulphur Auger peak at 152 eV, and the strongest of the high-energy KLL sulphur Auger peaks at ≈2117 eV.

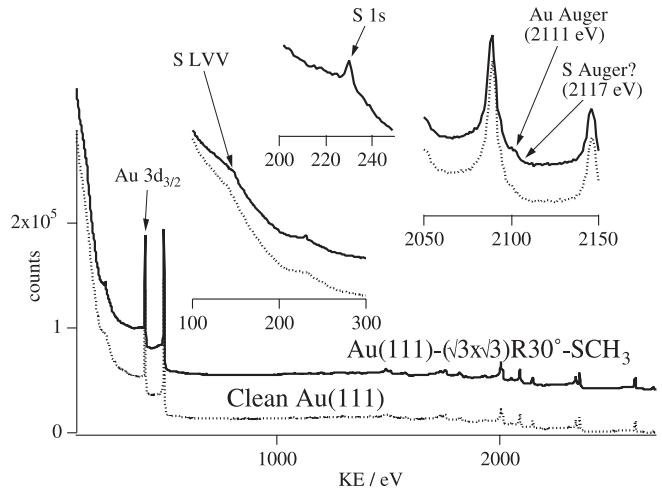

Figure 9. EDCs for clean Au(111) (dotted curves) and Au(111)-($\sqrt{3} \times \sqrt{3}$)$R30°$-SCH_3 (full curves) using an x-ray energy of 2700 eV. The insets show expanded sections of these EDCs illustrating where the S LVV Auger, S 1s photoelectron and S (2117 eV) Auger peaks lie.

At a nominal Au{111} NIXSW energy of 2630 eV the sulphur 2s and 2p photoelectron peaks can be eliminated as possibilities as their cross sections for photoionization at this energy are too small to make them visible in the spectrum. The low-energy LVV Auger cannot be used for two reasons. First, as has just been noted, the L (2s and 2p) levels have small photoionization cross sections at these energies, so the directly photo induced LVV Auger intensity will be weak. Second, the sulphur 2s and 2p core levels are sufficiently shallow in energy that they are easily ionized by the gold photoelectrons, gold Auger electrons and the secondary electrons with KEs >229 eV. As these gold derived electrons constitute almost the entire EDC, the L core hole concentration will be dominated by electron induced ionization processes rather than direct photoionization and the intensity of the LVV sulphur Auger peak therefore fluctuates in intensity in exactly the same way as the gold Auger electrons. This means that an XSW curve measured using the sulphur LVV Auger peak will look the same as the gold Auger derived curve, and so be of no use.

Third, the KLL sulphur Auger peak should be a good candidate for measuring the sulphur XSW curve, as the K level has a large photoionization cross section at this photon energy, and there are insufficient gold derived electrons at higher KEs to cause any appreciable ionization of the K level by gold-derived photo or Auger electrons. Unfortunately, as figure 9 shows, there are several gold Auger and photoelectron peaks in the vicinity of the sulphur KLL Auger peak, and it is only with great difficulty that the sulphur Auger peak can be unambiguously identified. The KLL Auger peak is therefore a poor candidate for measuring the sulphur XSW curve. Note the equivalent chlorine KLL Auger on Cu(111) could be used (above) because there were no copper substrate peaks nearby, and hence the Auger peak resided on a low-intensity, flat, featureless background of secondary electrons.

On examining the fourth and last possibility for monitoring the sulphur XSW curve, we find that the sulphur 1s photoelectron peak can be observed clearly on the low energy secondary electron background. However, figure 9 was taken using a photon energy of 2700 eV to ensure that the photoelectron peak is clearly visible. At the XSW energy of ≈2630 eV the S 1s photoelectron peak occurs at a KE of ≈160 eV, in the vicinity of the low energy LVV sulphur Auger (151 eV) and a whole range of weak gold Auger peaks (141, 150, 160, 165, 184 eV).

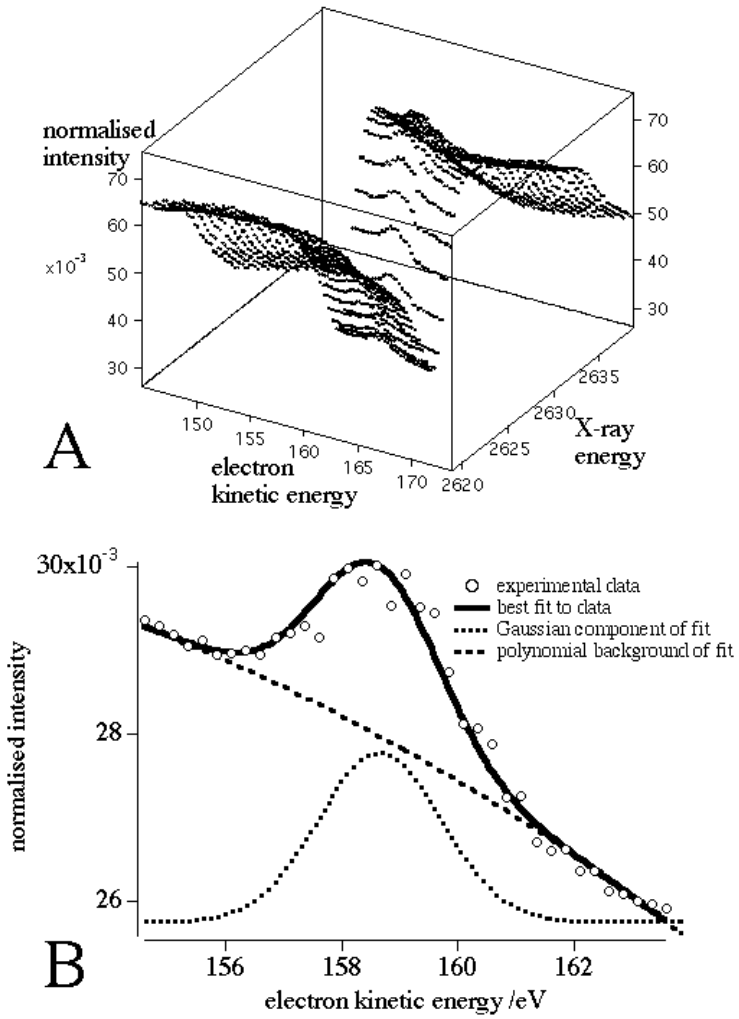

Figure 10. (a) A 3D plot showing the many small EDC scans taken across the S 1s photoelectron peak as the photon energy is scanned through the (111) XSW region for the Au(111)-$(\sqrt{3} \times \sqrt{3})R30^{\circ}$-$SCH_3$ surface. Notice the large modulation of the background, which has the characteristic gold XSW shape. (b) A typical fit to one of the EDCs using a polynomial to model the background, and a Gaussian for the S 1s photoelectron peak.

So during an XSW scan the sulphur 1s photoelectron peak passes over the sulphur Auger peak and some of the weaker gold Auger peaks, as well as moving down a very steep secondary electron background. Fortunately, all these features are broad in comparison to the rather sharp photoelectron peak, so although difficult, it is possible to separate the intensity of the S 1s peak from the underlying background of Auger and secondary electron peaks.

Figure 10(a) shows a complete NIXSW data set for methane thiolate on Au(111), where individual EDCs were obtained at each photon energy, the window of the EDC being moved to track the movement of the sulphur 1s photoelectron peak. Figure 10(b) shows how each EDC can be fitted using a polynomial background to mimic the slowly varying shape of the underlying Auger and secondary electron background, and a Gaussian profile to fit the shape

of the 1s photoelectron peak itself. From these fits, taken using the gold (111) and ($\bar{1}$11) reflections, the XSW profiles can be extracted and then fitted using non structural parameters (σ and E_0) transferred from XSW scans for the gold substrate, and the structural parameters of interest, d and f. This work is in progress at present and should provide a determination of the adsorption site of sulphur in methane thiolate on Au(111).

7. Conclusions

NIXSW analysis can be applied to a range of surface structural problems. It is exceedingly good at identifying the adsorption site for a range of adsorbates: for SiH_x on Cu(111) the adsorption site is the hcp 3-fold hollow while for $ClCH_2CH_2F$ on Cu(111) both halogens reside in atop sites. We have also shown that for elements exhibiting Auger peaks for which all three energy levels are relatively deep, the large chemical shift in the Auger peak may be easier to use in chemical shift XSW measurements than the smaller shift in the associated photoelectron peak. Finally we have shown how XSW data can be obtained for a particularly difficult system, sulphur on gold.

Acknowledgments

We would like to thank the EPSRC of Great Britain for supporting this work in the form of grants and access to the CLRC Daresbury Laboratory SRS, and providing studentships to JJL, MGR and GJJ. MPS and ASYC would like to thank the University of Nottingham for providing studentships and NKS the University of New South Wales for subbatical leave.

References

[1] Woodruff D P, Seymour D L, McConville C F, Riley C E, Crapper M D, Prince N P and Jones R G 1987 *Phys. Rev. Lett.* **58** 1460
[2] Zegenhagen J 1993 *Surface Sci. Rep.* **18** 199
[3] Woodruff D P 1998 *Prog. Surf. Sci.* **57** 1
[4] Wang J, Caffrey M, Bedzyk M J and Penner T L 1994 *J. Phys. Chem.* **98** 10 957
[5] Woodruff D P, Cowie B C C and Ettema A R H F 1994 *J. Phys.: Condens. Matter* **6** 10 633
[6] Curson N J, Bullman H G, Buckland J R and Allison W 1997 *Phys. Rev.* B **55** 10 819
[7] Shuttleworth I G, Fisher C J, Lee J J, Jones R G and Woodruff D P 2001 *Surf. Sci.* **491** L645
[8] Chan A S Y and Jones R G 2000 *Surf. Sci.* **451** 232
[9] Jones R G, Chan A S Y, Turton S, Jackson G J, Singh N K, Woodruff D P and Cowie B C C *J. Phys. Chem.* **105** 10 600
[10] Jackson G J, Cowie B C C, Woodruff D P, Jones R G, Kariapper M S, Fisher C, Chan A S Y and Butterfield M 2000 *Phys. Rev. Lett.* **84** 2346
[11] Lee J J, Fisher C J, Woodruff D P, Jones R G, Roper M G and Cowie B C C *Surf. Sci.* submitted
[12] Jackson G J, Lüdecke J, Woodruff D P, Chan A S Y, Singh N K, McCombie J, Jones R G, Cowie B C C and Formoso V 1999 *Surf. Sci.* **441** 515
[13] Jackson G J, Driver S M, Woodruff D P, Abrams N, Jones R G, Butterfield M, Crapper M D, Cowie B C C and Formoso V 2000 *Surf. Sci.* **459** 231
[14] Jones R G and Clifford C A 1999 *Phys. Chem. Chem. Phys.* **1** 5223
[15] Walter W K, Manolopoulos D E and Jones R G 1996 *Surf. Sci.* **348** 115
[16] Skegg M and Jones R G 2001 unpublished results
[17] McGuire G E 1979 *AES Reference Manual* (New York: Plenum)
[18] Coglan W A and Clausing R E 1973 *Atomic Data* **5** 317
[19] Moretti G 1998 *J. Electron Spectrosc. Rel. Phenomena* **95** 95
[20] Ulman A 1991 *An Introduction to Organic Films* (San Diego, CA: Academic)
[21] Dubois L H and Nuzzo R G 1992 *Ann. Rev. Phys. Chem.* **43** 437
[22] Fentner P, Schreiber F, Berman L, Scoles G, Eisenberger P and Bedzyk M J 1998 *Surf. Sci.* **412/413** 213